

## Effect of particle size on the oral absorption of isoliquiritigenin nanocrystals

Yanni Ma<sup>1,2#</sup>, Xiaoying Yang<sup>1,2#</sup>, Guoting Chen<sup>1</sup>,  
Yuxin Zhang<sup>1,2</sup>, Hao Zhang<sup>1,2</sup>, Wenping Zhang<sup>1,2\*</sup>

<sup>#</sup>The authors have contributed equally to this work.

<sup>1</sup>Department of Pharmacy, General Hospital of Ningxia Medical University, Yinchuan, China, <sup>2</sup>Institute of Clinical Pharmacology, Department of Pharmacy, General Hospital of Ningxia Medical University, Yinchuan, China

As one of the most promising formulations for poorly water-soluble drugs, nanocrystals have been attracting increasing attention in recent years. Isoliquiritigenin (ISL) is a flavonoid with a chalcone structure, and possesses many biological activities. However, its clinical application is significantly limited mainly due to its low oral bioavailability caused by poor hydrophilicity. To address this, ISL nanocrystals were developed in this study to improve its oral bioavailability. Three types of nanocrystals with differing particle size; R1, R2, and R3, were prepared by anti-solvent precipitation or anti-solvent precipitation combined with sonication, which was optimized by single-factor experiments. These nanocrystals were characterized based on their physical properties, in vitro release, and in vivo absorption performance. The mean particle size of R1, R2, and R3 was 555.7, 271.0, and 46.2, respectively. The dissolution ratio of ISL in the nanocrystals was significantly improved, with the quickest rate recorded in R2. Peak concentration and area under the concentration-time curve of R2 after oral administration in rats was 5.83- and 2.72-fold higher than that of the ISL solution, respectively. These findings indicate that the dissolution and absorption of ISL can be significantly enhanced by nanocrystals, and the dissolution behavior and pharmacokinetic properties of nanocrystals is significantly influenced by particle size.

**Keywords:** Isoliquiritigenin; Nanocrystals; Particle size; Oral bioavailability; HPLC-MS/MS.

### INTRODUCTION

Isoliquiritigenin (ISL), a flavonoid with a chalcone structure (2,4,4-trihydroxychalcone), is found in licorice, shallots, and bean sprouts (Zhang *et al.*, 2013). It has gained considerable attention due to its beneficial health effects including antioxidative, analgesic, anti-inflammatory activity, cytoprotective effects, antiplatelet aggregation, antiangiogenic effect, and radical scavenging activity (Kobayashi *et al.*, 1995; Peng *et al.*, 2015; Zhou, Wink, 2019). Recently, the antitumor activities of ISL have also attracted attention (Zhang *et al.*, 2013). ISL has been reported to inhibit the proliferation of many different types

of cancer cells, and reduce the growth and metastasis of hepatocellular carcinoma (Wang *et al.*, 2019), colon cancer (Yoshida *et al.*, 2008), gastric cancer (Zhang *et al.*, 2018), breast cancer (Lee *et al.*, 2015), prostate cancer (Kwon *et al.*, 2009), endometrial cancer (Wu *et al.*, 2016), and lung cancer cells (Jung *et al.*, 2014; Zhang, Zhang, Ni, 2019). In particular, inhibition of tumor cell proliferation is at least partially achieved by blocking the tumor cell cycle at the G2/M phase via the upregulation of p53, p21, and GADD153 in Hep G2 hepatoma cells, DU145 and LNCaP prostate cancer cells, and A549 human lung cancer cells and uterine leiomyoma cells, respectively (Hsu *et al.*, 2005; Kanazawa *et al.*, 2003). Furthermore, topoisomerase II activity and metaphase/anaphase transition have been shown to be inhibited and blocked in HeLa cells (Kanazawa *et al.*, 2003). Moreover, topoisomerase II activity and metaphase/anaphase transition were inhibited and blocked in HeLa

\*Correspondence: W. Zhang. Department of Pharmacy. Institute of Clinical Pharmacology. General Hospital of Ningxia Medical University, Yinchuan, China. Phone: +86-0951-6743430. E-mail: zhangwenping2008bs@163.com. ORCID: <https://orcid.org/0000-0002-3905-3332>

cells (Park *et al.*, 2009). However, the absorption of ISL is limited by its poor solubility (Lee *et al.*, 2013). It has been reported that the solubility of ISL can be improved by using a nanostructured lipid carrier (Zhang *et al.*, 2013).

There are many methods presently used to improve the solubility of water-insoluble drugs, such as cosolvent solubilization, inclusion complexes, emulsion, microemulsion, and solid dispersion technology (Patel, Zode, Bansal., 2020). However, these methods have some limitations such as cosolvent organic solvent toxicity and compatibility with drug problems for precipitation. Additionally, inclusion complexes require specific-sized drug molecules and cyclodextrin, which may increase the drug burden on patients with kidney disease (Liu *et al.*, 2021a). Emulsion dispersion technology requires a high solubility of the drug in the oil phase; therefore, some insoluble compounds are still suitable.

Nanocrystals are defined as submicron colloidal dispersions of nanosized drug particles and comprise stabilizers, surfactants, or a mixture of both, and drugs (Patravale, Date, Kulkarni, 2004). Nanocrystals can be prepared by this method regardless of whether the drug is insoluble in water or oil (Liu *et al.*, 2021b). Furthermore, they are easy to produce on a large scale at low cost. They are mainly applied to oral drug delivery, and other drug delivery routes, such as oral, injection, ocular, and lung delivery (Yang *et al.*, 2018). Recently, nanocrystals have been widely used to improve the solubility and bioavailability of poorly water-soluble drugs through a reduction in drug particle size. Some of the stabilizers presented in a nanocrystal formulation show a solubilizing effect, which might further enhance the *in vivo* absorption of a drug (Gao *et al.*, 2013; Tuomela, Hirvonen, Peltonen, 2016). In addition, nanocrystals have a high drug loading and can effectively reduce the drug delivery volume, improving patient compliance and lowering risk (Gol, Thakkar, Misra, 2018; Pardhi *et al.*, 2018). Moreover, nanocrystals can also increase the physical and chemical stability of drugs. It has been widely reported that when intravenously administered, nanosuspensions can target tumor sites through an enhanced permeability and retention effect (Hong *et al.*, 2017). Therefore, nanocrystal technology could be a suitable strategy for enhancing the solubility and oral bioavailability of ISL.

In the present study, ISL nanocrystals were prepared using an anti-solvent precipitation method and optimized by single-factor experiments to obtain different particle-sized ISL nanocrystals. The effects of particle size on the *in vitro* release and *in vivo* pharmacokinetics of the drug nanocrystals were investigated and compared.

## MATERIAL AND METHODS

### Materials

ISL (purity 98%) and curcumin (CUR, purity 98%) were provided by Jingzhu Biological Technology Co., Ltd. (Nanjing, China). methoxyl polyethylene glycol (mPEG)2000-polycaprolactone (PCL) (Mw, 1,140, 2,000, 4,000, 5,300, 6,000, 8,000, and 10,000) and mPEG5000-PCL (Mw, 1000, 2000, 4000, 5,000, 10,000, 15,000, 20,000, and 45,000) were purchased from Daigang Biotechnology Engineering Co. (Jinan, China). Polyvinyl pyrrolidone K30 was obtained from Hayashibara Co., Ltd. (Henan, China). Ethanol (analytical grade) was acquired from Damao Chemical Industry Co. (Tian jin, China). Methanoic acid (chromatographic grade) was acquired from Damao Chemical Industry Co. (Tian jin, China). Methanol and acetonitrile (chromatographic grade) were supplied by Fisher Co., Ltd. (Fair lawn, USA). Double-distilled water for all experiments was prepared by a Milli-Q Plus integral water purification system (Millipore, Darmstadt, Germany). All other reagents were of analytical grade.

### Preparation of ISL nanocrystals

ISL nanocrystals were prepared using an anti-solvent precipitation method or in combination with an ultrasonication process according to a previous study (Chang *et al.*, 2018). First, 20 mg ISL was completely dissolved in 1 mL ethanol to obtain a concentrated drug solution of 20 mg/mL. An aqueous solution was prepared using surfactants as a stabilizer. The surfactants were dissolved in 10 mL double-distilled water to form the aqueous solution. Then, 1 mL 20 mg/mL ISL solution was rapidly injected into the aqueous solution under rapid stirring (Yuhua Apparatus Co., Gongyi, China) at room temperature. Finally, the mixed solution was

sonicated by a XO-650 ultrasonic processor (Xian'ou Instruments Manufacturing Co., Ltd. Nanjing, China) at 260 W for 1 h in an ice-water bath. The nanocrystals were then extruded through a 0.45- $\mu\text{m}$  polyamide filter (Yibo Filtering Equipment Factory, Haining, China). ISL nanocrystals produced from mPEG2000-PCL1140, mPEG2000-PCL2000, and mPEG5000-PCL5000 were named R1, R2, and R3, respectively.

### Particle size analysis

The mean particle size and polydispersity index (PDI) of each ISL nanocrystal formulation was determined by dynamic light scattering analysis in a Zetasizer Nano-ZS90 (Malvern Instruments, Malvern, UK) at 25 °C. All analyses were measured in triplicate.

### Morphology observation

The morphology of the ISL nanocrystals was observed via a transmission electron microscopy (TEM) instrument (H-7500, Hitachi Ltd, Tokyo, Japan). A drop of ISL nanocrystals was stained with 2% phosphotungstic acid and deposited on the surface of copper grids. The samples were then air-dried and examined by TEM.

### HPLC analysis of ISL

ISL concentration was determined by a high-performance liquid chromatography (HPLC) system (Agilent 1200, USA) with a UV detector (292 nm). The chromatographic separations were achieved using an Agilent Eclipse XDB-C18 column (250 mm $\times$ 4.6 mm, pore size 5  $\mu\text{m}$ ) at 30°C. The mobile phase consisted of a 45:55 (v/v) mixture of acetonitrile:0.04% formic acid at a flow rate of 1.0 mL/min. The calibration curve of ISL was linear over the range of 0.25–100  $\mu\text{g}/\text{mL}$  with  $R^2 > 0.9999$ , and no interference was observed with mPEG-PCL at 292 nm.

### HPLC-MS/MS analysis of ISL

ISL pharmacokinetics was investigated by HPLC-tandem mass spectrometry (MS/MS). HPLC-MS/MS

utilized a LC-30A (Shimadzu, Japan) and the column effluent was monitored by an API4000 triple quadrupole mass spectrometer (Applied Biosystems, Concord, Canada) equipped with an electrospray ionization source. Chromatographic separations were performed on a Shim-pack XR-ODS column (2.0 mm $\times$ 100 mm, pore size 3  $\mu\text{m}$ , Shimadzu) maintained at 40 °C. The mobile phase was an isocratic elution, which included acetonitrile and 0.1% formic acid (60:40, v/v). The flow rate was 0.3 mL/min, and the sample injection volume was 5  $\mu\text{L}$ . The ion spray voltage was set at  $-4,500$  V. Compound parameters viz, declustering potential, collision energy, entrance potential, and collision exit potential were  $-55$ ,  $-23$ ,  $-10$ , and  $-12$  V for CUR, respectively, and  $-70$ ,  $-34$ ,  $-10$ , and  $-12$  V for ISL, respectively. The mass spectrometer was operated in the electrospray ionization negative ion mode, and ion detection was performed in the multiple reaction monitoring mode, monitoring the transition of the  $m/z$  367.2 precursor ion  $[\text{M}-\text{H}]^-$  to the  $m/z$  148.9 product ion for CUR, and the  $m/z$  256.5 precursor ion  $[\text{M}-\text{H}]^-$  to the  $m/z$  136.9 product ion for ISL.

### In vitro release of ISL nanocrystals

The in vitro release of ISL from the nanocrystal formulations was analyzed by membrane dialysis against 0.1% sodium dodecylsulphate at 37 °C. Briefly, a 1 mL aliquot of ISL nanocrystals was placed in the dialysis tube (Green Bird Science dialysis tubes with a Mw cutoff of 14,000 Da) and then suspended in an Erlenmeyer flask containing 149 mL of 0.1% sodium dodecylsulphate. The flask was then placed in a water bath shaker (SHA-C, Hualong Experimental Apparatus Industry, China), which was maintained at 37 °C and shaken horizontally at 100 rpm. At 0.5, 1, 1.5, 2, 2.5, 3, 3.5, 4, 5, 6, 8, 10, 12, 24, and 48 h, a 2 aliquot mL was withdrawn from the flask and replaced with the same amount of fresh release medium. The concentration of ISL was assayed by HPLC.

### Solubility

To measure ISL and nanocrystal solubility, 20 mg of ISL was dissolved in 10 mL of water, filtered through a 0.45-

$\mu\text{m}$  filter membrane, and the concentrations of drugs in the filtrate and different nanocrystals were then determined.

### Stability

The prepared nanocrystals were placed in a refrigerator at 4 °C, and the changes in particle size and encapsulation efficiency at 0 and 20 days were measured.

### Pharmacokinetic study in rats

A total of 24 healthy adult male Sprague-Dawley rats ( $220 \pm 20$  g) were provided by the Laboratory Animal Center of Ningxia Medical University (Yinchuan, China). All procedures were approved by the Animal Research Ethics Committee, General Hospital of Ningxia Medical University. The rats were maintained in a specific pathogen-free environment that was temperature-controlled ( $23 \pm 2$  °C) with free access to water, and were fasted for 12 h before experimentation. They were then randomly divided into four groups to receive oral administration of either the ISL suspension (control group), R1, R2, or R3, each at a dose of 30 mg/kg body

weight. Plasma samples of 0.5 mL were obtained from orbital veins and transferred into heparinized tubes at 5, 10, 20, and 30 min, and at 1, 1.5, 2, 3, 4, 6, 8, 10, and 24 h after administration. All blood samples were separated immediately by centrifugation at 3,500 rpm- for 5 min and kept frozen at  $-80$  °C until analysis. Then, 50  $\mu\text{L}$  of plasma was added to 10  $\mu\text{L}$  CUR (Internal standard, IS) and 300  $\mu\text{L}$  acetonitrile to precipitate protein. After vortexing for 5 min, the mixture was centrifuged at 14000 rpm for 10 min. The supernatant was collected and then directly measured. The concentration of ISL in the plasma was determined using a validated LC-MS assay.

Pharmacokinetic parameters were measured using a non-compartmental model with the DAS 3.0 software package (Bojia Corp., Shanghai, China). The various pharmacokinetic parameters analyzed included peak concentration ( $C_{\text{max}}$ ), time to reach  $C_{\text{max}}$  ( $T_{\text{max}}$ ), and area under the concentration-time curve. The results were expressed as the mean and standard deviation (SD). One-way analysis of variance (ANOVA) was used to analyze the data using SPSS software (version 17.0, IBM®, Chicago, IL USA). P-values less than 0.05 were considered statistically significant.

## RESULTS AND DISCUSSION

### Preparation of different particle-sized ISL nanocrystals

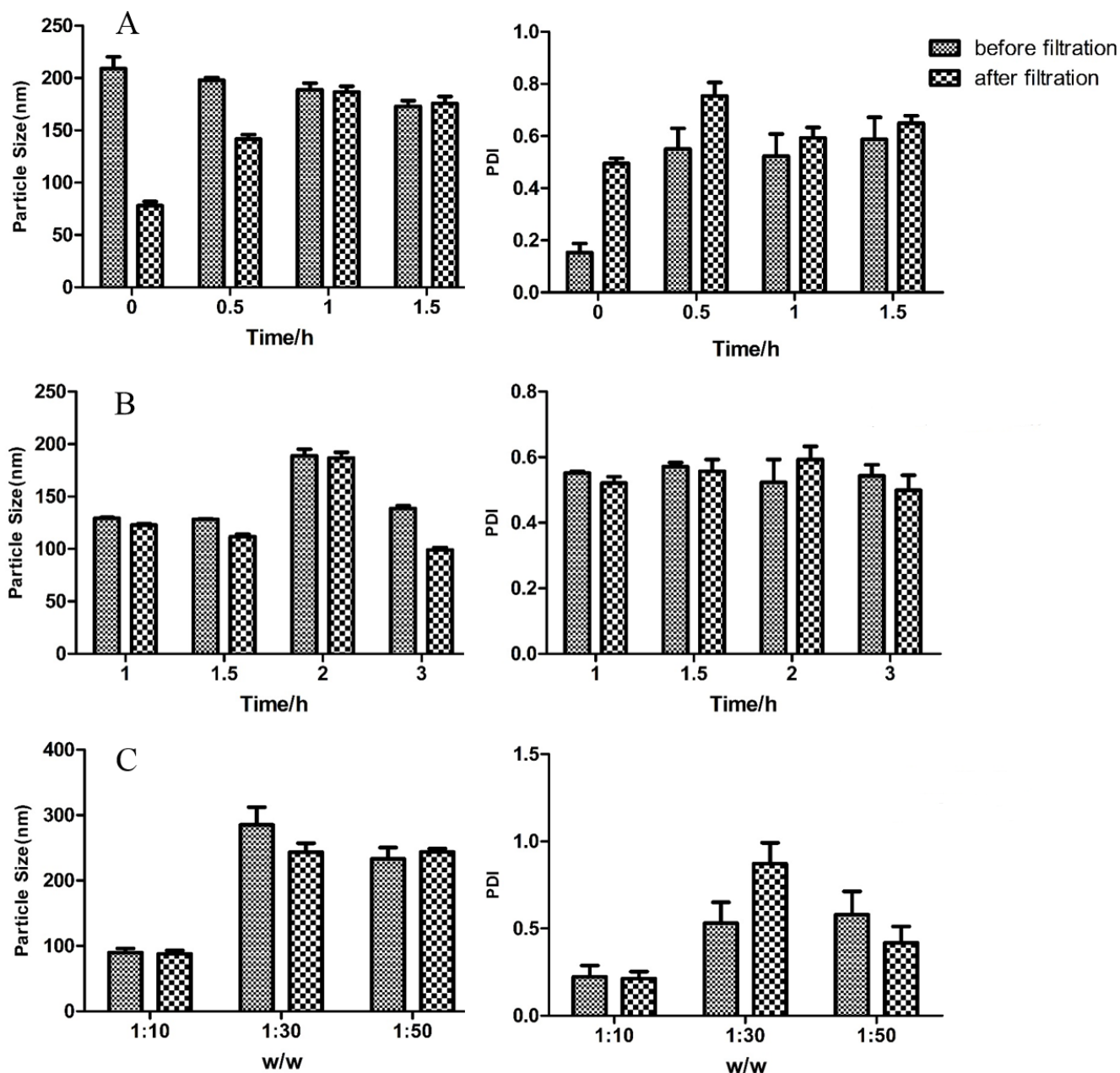


**FIGURE 1** - Effect of ultrasonication time (A), stirring time (B), and solvent ratio (C) on particle size and PDI (mean  $\pm$  SD, n = 3).

According to the results of the single-factor experiments, the optimized formulation was as follows: ratio of organic phase and aqueous phase = 1:10, ultrasonication time = 1 h, and stirring time = 1 h. As

shown in Figure 1, the secondary growth of nanocrystals could be effectively avoided by ultrasound after stirring, and particle aggregation could be prevented, which played a vital role in achieving nanocrystal stability. As the

proportion of aqueous phase increased, the nanocrystal system became turbid, and precipitation was obvious after placement. When the solvent proportion was 1:10, nanocrystals particle size and distribution was stable before and after filtration. In order to prepare different particle-

sized ISL nanocrystals, mPEG-PCL preparations of differing chain lengths were selected. The concentrations of mPEG2000-PCL1140, mPEG2000-PCL2000, and mPEG5000-PCL5000 in an aqueous solution were 40%, 14%, and 14% (w/v), respectively (Table I).

**TABLE I** - Process parameters for the preparation of different particle-sized ISL nanocrystals

Sample	Process parameters surfactant concentrations in aqueous phase(%)	Sonicated or not Sonicated	Mean particle sizes (nm) $\pm$ SD	PDI
R1	40%	Unsonicated	555.7 $\pm$ 15.1	0.16 $\pm$ 0.12
R2	14%	Sonicated at 400W for 1h	271.0 $\pm$ 16.3	0.11 $\pm$ 0.04
R3	14%	Sonicated at 400W for 1h	46.2 $\pm$ 0.04	0.14 $\pm$ 0.01

### Characterization of ISL nanocrystals

As shown in Figure 2, the particle size of R1, R2, and R3 was 542.1, 272.8, and 46.22 nm, respectively, and the PDI was 0.024, 0.085, and 0.127, respectively. However, the particle size and PDI of the ISL solution was 1,182 nm and 0.517, respectively. The particle size of the nanocrystals decreased significantly compared

with that of the solution. The nanocrystals possessed different physicochemical characteristics. They were nearly spherical in shape and uniformly distributed; the mean diameter of PEG and PCL nanoparticles with different chain lengths was in the range of 40–600 nm.

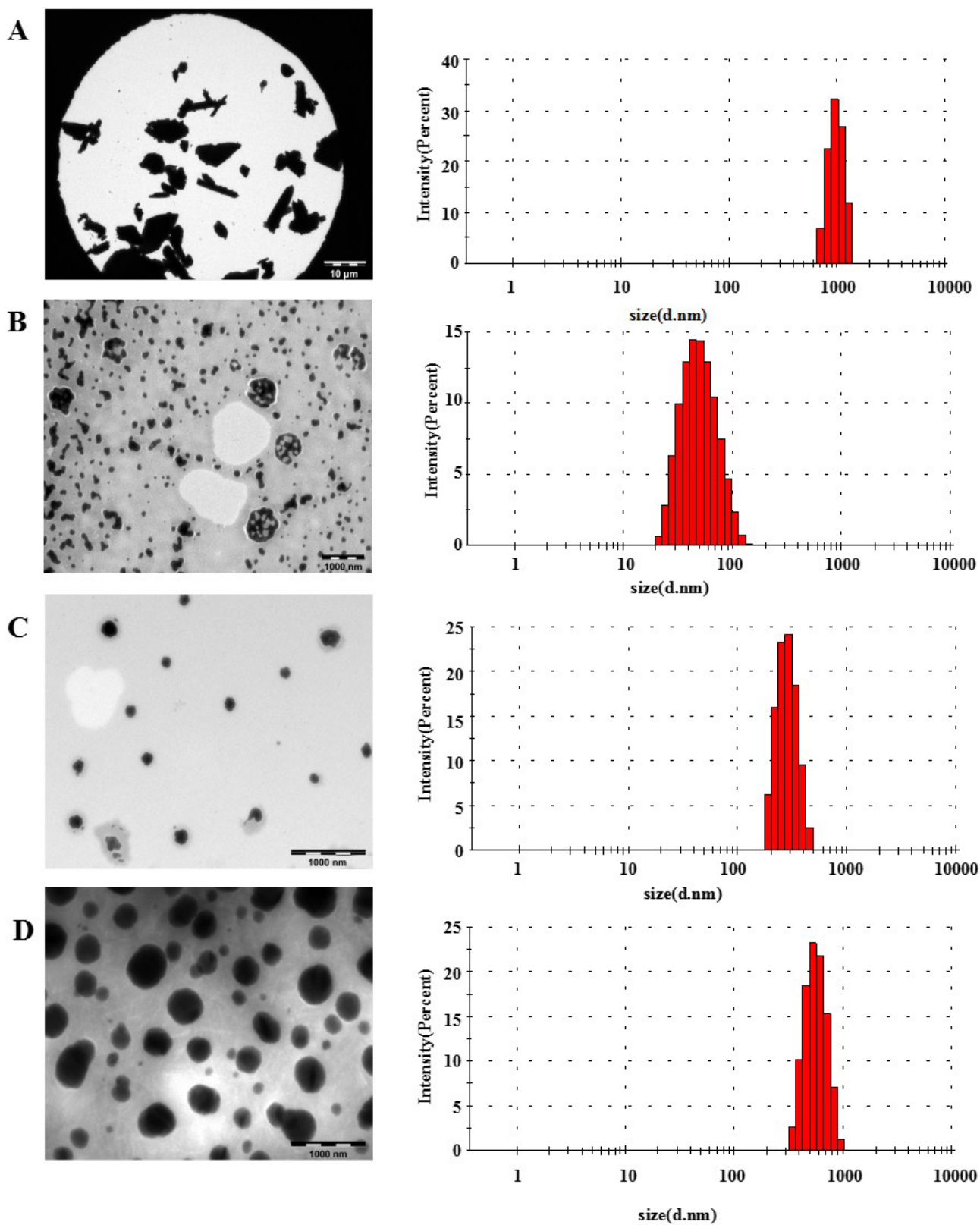


**FIGURE 2** - Particle size distribution and TEM images of the ISL solution (A), R3 (B), R2 (C), and R1 (D).

## In vitro drug release

The drug release performances of R1, R2, R3, and the ISL solution were investigated and are shown in Table II and Figure 3. The dissolution velocities of R1, R2, and R3 were distinctly superior compared to the ISL solution. R1, R2, and R3 released 71.81%, 87.62%, and 80.89% within 48 h, respectively. However, only 31.29% of the coarse ISL solution dissolved within 48 h. Compared to the coarse ISL solution, R1, R2, and R3 showed a significantly improved dissolution performance (one-way ANOVA,  $p < 0.001$ ), with the R2 formulation being the most superior. This suggests that nanocrystal technology could markedly increase the dissolution rate of ISL. Meanwhile, a reduction of particle size could increase the dissolution velocity of

nanocrystals; however, a smaller size was not better, only when the particle size was approximately 300 nm, the dissolution velocity was the fastest. Additionally, there were significant effects of different hydrophobic and hydrophilic chain lengths, and the ratio of the hydrophilic to hydrophobic segment on ISL release. These results reveal that the formation of nanocrystals strongly enhances the dissolution rate and extent of ISL, partly due to the existence of formulation surfactants such as mPEG, but mostly explained by the large reduction in particle size via nanocrystal technology (Gan *et al.*, 2017). Additionally, three different physical mixtures were formulated and compared with the prepared samples. The cumulative release curves of these are shown in Figure 3. These findings indicate that there was no effect of the excipients on the dissolution.

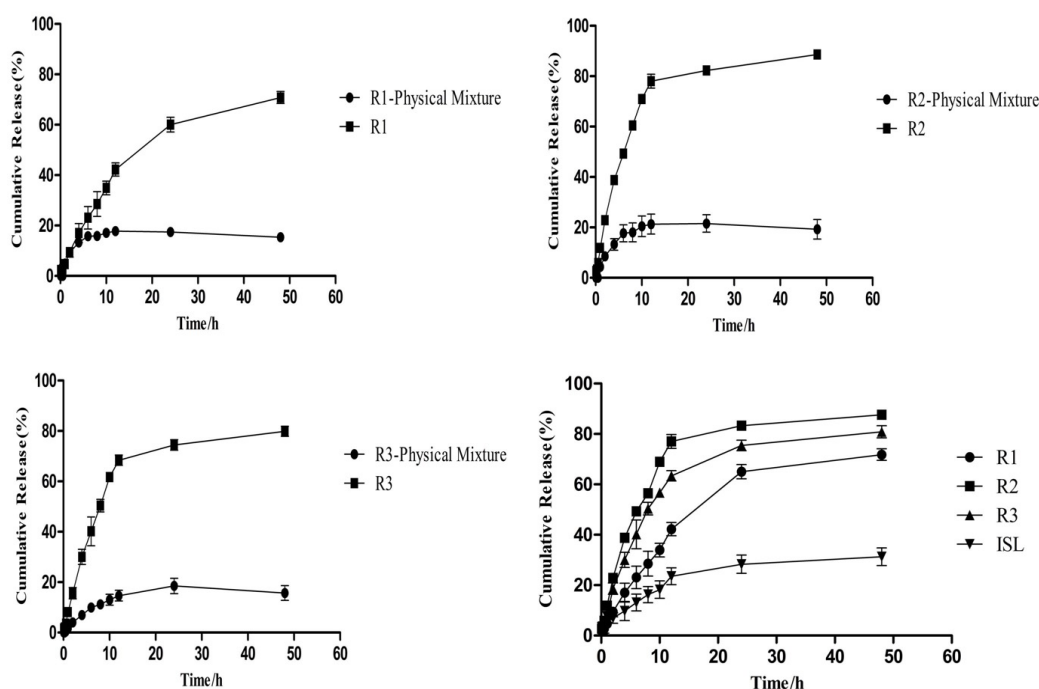


**FIGURE 3** - In vitro release curve of the ISL nanocrystal physical mixtures R1 (mPEG2000-PCL1140), R2 (mPEG2000-PCL2000), and R3 (mPEG5000-PCL5000), and the ISL solution in 0.1% SDS (mean  $\pm$  SD,  $n = 3$ ).

## Solubility

The drug concentration in the filtrate was  $0.07 \pm 0.00$   $\mu\text{g/mL}$ , almost water-insoluble. However, the concentration

of nanocrystals R1, R2, and R3 prepared from the same quality drug was  $1,901.78 \pm 6.06$   $\mu\text{g/mL}$ ,  $1,903.73 \pm 5.31$   $\mu\text{g/mL}$ , and  $1,908.17 \pm 7.17$   $\mu\text{g/mL}$ , respectively. Drug solubility significantly increased with nanoparticle production.

## Stability

Stability was checked by the encapsulation efficiency and particle size of the nanocrystals after 20 days at 4 °C in the refrigerator, as shown in Table II and Figure 3. The

variation range of encapsulation efficiency and particle size before and after storage was within 3%, and there was no precipitation in the preparations, indicating that the nanocrystals were relatively stable.

**TABLE II** - Encapsulation efficiency and particle size of the nanocrystals after 20 days at 4 °C

	Encapsulation efficiency (%) ± SD			Mean particle sizes (nm) ± SD	
	0d	20d	0d	20d	
R1	95.09±0.30	92.29±1.98	548.3±2.40	535.7±13.93	
R2	95.19±0.27	92.24±0.84	263.0±1.36	257.6±3.08	
R3	95.41±0.36	93.62±1.98	57.62±1.31	56.03±2.03	

## Pharmacokinetic study in rats

To further confirm the advantage of an ISL nanocrystal formulation, the in vivo pharmacokinetic performance of the ISL nanocrystals was studied in Sprague Dawley rats and compared to that of the coarse ISL solution. The ISL blood concentration-time curves after oral administration of the different formulations are shown in Figure 4, and the pharmacokinetic parameters are listed in Table III. As shown in Figure 4, all nanocrystals formulation significantly improved the oral absorption of ISL. This was also indicated by the results in Table III; the three nanocrystal formulations reached maximum plasma drug concentration at approximately 15 min; however, the  $C_{max}$  and area under the concentration-time curve values of R2 were 5.83- and 2.72-fold higher than those of the coarse ISL solution, respectively. Compared to the coarse ISL solution, R1, R2, and R3 showed a significantly improved dissolution performance (one-way ANOVA,  $p < 0.05$ ), with the R2 formulation

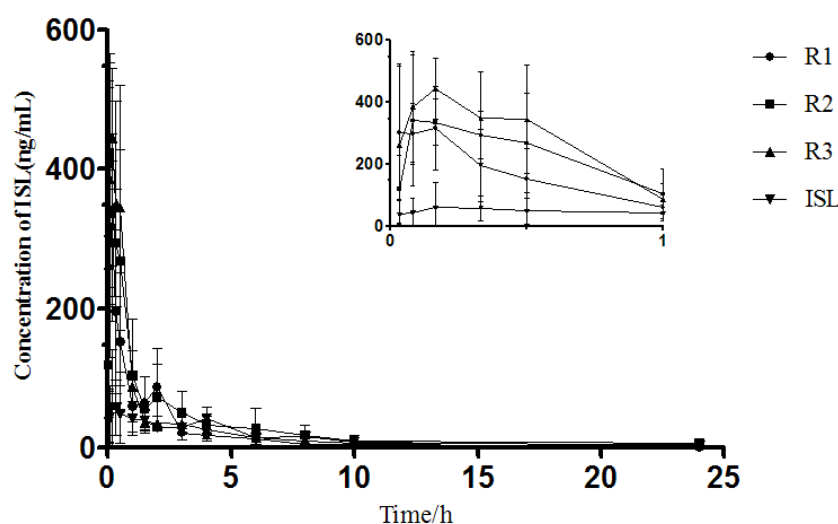
being the most superior. This indicated that nanocrystals of 300 nm particle size can significantly enhance the drug concentration in the blood vs drug solution. However, smaller particle sizes were not the best. The clearance data showed that the coarse ISL solution was quickly removed from the circulation system, while R2 represented a markedly delayed blood clearance due to a sustained release ( $p < 0.01$ ). Moreover, the differences in apparent distribution volume between the nanocrystals and coarse ISL solution were not significant ( $p > 0.05$ ). These results were consistent with those obtained in the in vitro drug release experiment.

Overall, these data demonstrate that the nanoparticles R2, 300 nm in particle size, significantly improved the AUC and  $C_{max}$ , and decreased the clearance compared to the coarse ISL solution. ISL nanocrystal particle size had a significant effect on the pharmacokinetic properties in vivo. Therefore, in order to achieve the desired therapeutic purpose, it is very important to screen the optimal particle size of the nanocrystals.

**TABLE III** - Pharmacokinetic parameters following oral administration of the ISL solution and ISL nanocrystals (mean  $\pm$  SD, n = 6)

Parameter	Coarse ISL	R1	R2	R3
$C_{max}$ (ng/ml)	97.92 $\pm$ 74.74	460.67 $\pm$ 84.90**	571.17 $\pm$ 209.77***	488.50 $\pm$ 177.36**
$T_{max}$ (h)	0.96 $\pm$ 1.53	0.15 $\pm$ 0.11	0.19 $\pm$ 0.16	0.24 $\pm$ 0.21
$AUC_{0-t}$ (ng·h/ml)	263.31 $\pm$ 93.75	423.34 $\pm$ 91.53*	717.35 $\pm$ 157.29***##	540.65 $\pm$ 120.67**※
$T_{1/2}$ (h)	4.06 $\pm$ 3.02	2.24 $\pm$ 0.36	2.48 $\pm$ 0.53	2.69 $\pm$ 1.40
$MRT_{0-t}$ (h)	3.59 $\pm$ 0.57	1.89 $\pm$ 0.89	4.28 $\pm$ 2.20#	2.97 $\pm$ 1.17
V(L/kg)	0.38 $\pm$ 0.08	0.18 $\pm$ 0.05	0.18 $\pm$ 0.16	0.23 $\pm$ 0.19
CL(L·kg/h)	0.08 $\pm$ 0.04	0.05 $\pm$ 0.01	0.03 $\pm$ 0.01**	0.04 $\pm$ 0.01*

\*p < 0.05 with respect to the coarse ISL suspension, #p < 0.05 with respect to R1, and ※p < 0.05 with respect to R2.

**FIGURE 4** - Plasma concentration-time curves of the ISL solution and ISL nanocrystals R1 (mPEG2000-PCL1140), R2 (mPEG2000-PCL2000), and R3 (mPEG5000-PCL5000) in Sprague Dawley rats after oral administration (mean  $\pm$  SD, n = 6).

## CONCLUSION

In this study, different particle-sized ISL nanocrystals were successfully prepared by a simple anti-solvent precipitation method and optimized with single-factor experiments. The obtained nanocrystals were morphologically characterized by a spherical shape. ISL in the nanocrystal formulations showed a significantly enhanced aqueous solubility and dissolution rate in vitro. The particle size of

ISL nanocrystals had a significant effect on the dissolution and pharmacokinetics in vitro and in vivo. The pharmacokinetic study indicated that the R2 nanocrystal formulation greatly improved drug absorption in rats after oral administration. These findings reveal that drug nanocrystal technology is a promising approach for enhancing the oral bioavailability of ISL. Moreover, they highlight the importance of optimizing an appropriate nanocrystal particle size regarding therapeutic purpose.

## ETHICAL STANDARDS

The experiments complied with the current laws of the country in which they were performed.

## DISCLOSURE STATEMENT

The authors report no conflicts of interest.

## STATEMENT OF ANIMAL RIGHTS

All institutional and national guidelines for the care and use of laboratory animals were followed.

## FUNDING

This work was financially supported from the Nature Science Foundation of Ningxia province (2020AAC03363), and National Nature Science Foundation Incubation Project of General Hospital of Ningxia Medical University in 2022.

## REFERENCES

Chang DC, Ma YN, Cao GY, Wang JH, Zhang X, Feng J, et al. Improved oral bioavailability for lutein by nanocrystal technology: formulation development, in vitro and in vivo evaluation. *Artif Cells Nanomed Biotechnol.* 2018;46(5):1018-1024.

Gan MY, Zhang WP, Wei SJ, Dang HW. The influence of mPEG-PCL and mPEG-PLGA on encapsulation efficiency and drug-loading of SN-38NPs. *Artif Cells Nanomed Biotechnol.* 2017;45(2):389-397.

Gao L, Liu GY, Ma JL, Wang XQ, Zhou L, Li X, et al. Application of drug nanocrystal technologies on oral drug delivery of poorly soluble drugs. *Pharm Res.* 2013;30(2):307-24.

Gol D, Thakkar S, Misra M. Nanocrystal-based drug delivery system of risperidone: lyophilization and characterization. *Drug Dev Ind Pharm.* 2018;44(9):1458-1466.

Hong JY, Liu YY, Xiao Y, Yang XF, Su WJ, Zhang MZ, et al. High drug payload curcumin nanosuspensions stabilized by mPEG-DSPE and SPC: in vitro and in vivo evaluation. *Drug Deliv.* 2017;24(1):109-120.

Hsu YL, Kuo PL, Lin CC. Isoliquiritigenin induces apoptosis and cell cycle arrest through p53-dependent pathway in Hep G2 cells. *Life Sci.* 2005;77(3):279-92.

Jung SK, Lee MH, Lim DY, Kim JE, Singh P, Lee SY, et al. Isoliquiritigenin induces apoptosis and inhibits xenograft tumor growth of human lung cancer cells by targeting both wild type and L858R/T790M mutant EGFR. *J Biol Chem.* 2014;289(52):35839-48.

Kanazawa M, Satomi Y, Mizutani Y, Ukimura O, Kawauchi A, Sakai T, et al. Isoliquiritigenin inhibits the growth of prostate cancer. *Eur Urol.* 2003;43(5):580-6.

Kobayashi S, Miyamoto T, Kimura I, Kimura M. Inhibitory effect of isoliquiritigenin, a compound in licorice root, on angiogenesis in vivo and tube formation in vitro. *Biol Pharm Bull.* 1995;18(10):1382-6.

Kwon GT, Cho HJ, Chung WY, Park KK, Moon A, Park JHY. Isoliquiritigenin inhibits migration and invasion of prostate cancer cells: possible mediation by decreased JNK/AP-1 signaling. *Biofactors. J Nutr Biochem.* 2009;20(9):663-76.

Lee SK, Park KK, Kim KR, Kim HJ, Chung WY. Isoliquiritigenin inhibits metastatic breast cancer cell-induced receptor activator of nuclear factor kappa-B ligand/osteoprotegerin ratio in human osteoblastic cells. *J Cancer Prev.* 2015;20(4):281-6.

Lee YK, Chin YW, Bae JK, Seo JS, Choi YH. Pharmacokinetics of isoliquiritigenin and its metabolites in rats: low bioavailability is primarily due to the hepatic and intestinal metabolism. *Planta Med.* 2013;79(17):1656-65.

Liu Y, Lin T, Cheng C, Wang Q, Lin S, Liu C, et al. Research Progress on Synthesis and Application of Cyclodextrin Polymers. *Molecules.* 2021a;26(4):1090.

Liu Z, Hu M, Zhang S, Jiang L, Xie F, Li Y. Oil-in-water Pickering emulsion stabilization with oppositely charged polysaccharide particles: chitin nanocrystals/fucoidan complexes. *J Sci Food Agric.* 2021b;101(7):3003-3012.

Pardhi VP, Verma T, Flora SJS, Chandasana H, Shukla R. Nanocrystals: an overview of fabrication, characterization and therapeutic applications in drug delivery. *Curr Pharm Des.* 2018;24(43):5129-5146.

Park I, Park KK, Park JHY, Chung WY. Isoliquiritigenin induces G2 and M phase arrest by inducing DNA damage and by inhibiting the metaphase/anaphase transition. *Cancer Lett.* 2009;277(2):174-81.

Patel D, Zode SS, Bansal AK. Formulation aspects of intravenous nanosuspensions. *Int J Pharm.* 2020;586:119555.

Patravale VB, Date AA, Kulkarni RM. Nanosuspensions: a promising drug delivery strategy. *J Pharm Pharmacol.* 2004;56(7):827-40.

Peng F, Qiaohui D, Cheng P, Wang N, Tang H, Xie X, et al. A review: the pharmacology of isoliquiritigenin. *Phytother Res.* 2015;29(7):969-77.

Tuomela A, Hirvonen J, Peltonen L. Stabilizing Agents for Drug Nanocrystals: Effect on Bioavailability. *Pharmaceutics.* 2016;8(2):16.

Wang JR, Luo YH, Piao XJ, Zhang Y, Feng YC, Li JQ, et al. Mechanisms underlying isoliquiritigenin-induced apoptosis and cell cycle arrest via ROS-mediated MAPK/STAT3/NF- $\kappa$ B pathways in human hepatocellular carcinoma cells. *Drug Dev Res.* 2019;80(4):461-470.

Wu CH, Chen HY, Wang CW, Shieh TM, Huang TC, Lin LC, et al. Isoliquiritigenin induces apoptosis and autophagy and inhibits endometrial cancer growth in mice. *Oncotarget.* 2016;7(45):73432-73447.

Yang H, Kim H, Jung S, Seo H, Nida SK, Yoo SY, et al. Pharmaceutical Strategies for Stabilizing Drug Nanocrystals. *Curr Pharm Des.* 2018; 24(21):2362-2374.

Yoshida T, Horinaka M, Takara M, Tsuchihashi M, Mukai N, Wakada M, et al. Combination of isoliquiritigenin and tumor necrosis factor-related apoptosis-inducing ligand induces apoptosis in colon cancer HT29 cells. *Environ Health Prev Med.* 2008;13(5):281-7.

Zhang XR, Wang SY, Sun W, Wei C. Isoliquiritigenin inhibits proliferation and metastasis of MKN28 gastric cancer cells by suppressing the PI3K/AKT/mTOR signaling pathway. *Mol Med Rep.* 2018;18(3):3429-3436.

Zhang XY, Qiao H, Ni JM, Shi YB, Qiang Y. Preparation of isoliquiritigenin-loaded nanostructured lipid carrier and the in vivo evaluation in tumor-bearing mice. *Eur J Pharm Sci.* 2013;49(3):411-422.

Zhang Y, Zhang R, Ni HJ. Eriodictyol exerts potent anticancer activity against A549 human lung cancer cell line by inducing mitochondrial-mediated apoptosis, G2/M cell cycle arrest and inhibition of m-TOR/PI3K/Akt signalling pathway. *Arch Med Sci.* 2019;16(2):446-452.

Zhou JX, Wink M. Evidence for anti-inflammatory activity of isoliquiritigenin, 18 $\beta$  glycyrrhetic acid, ursolic acid, and the traditional chinese medicine plants *glycyrrhiza glabra* and *eribotrya japonica*, at the molecular level. *Medicines.* 2019;6(2):55.

Received for publication on 31<sup>st</sup> December 2020

Accepted for publication on 19<sup>th</sup> October 2021